Arabian Journal of Chemistry (2022) **15**, 103603

King Saud University

Arabian Journal of Chemistry

www.ksu.edu.sa
www.sciencedirect.com

ORIGINAL ARTICLE

Sodium and potassium silicate-based catalysts prepared using sand silica concerning biodiesel production from waste oil

Keverson G. de Oliveira [a,*], Ramoni R.S. de Lima [a], Clenildo de Longe [a], Tatiana de C. Bicudo [b], Rafael V. Sales [a], Luciene S. de Carvalho [a,*]

[a] *Energetic Technologies Research Group, Institute of Chemistry, Federal University of Rio Grande do Norte, Natal 59078-970, Brazil*
[b] *Laboratory of Chemical Technology/School of Science and Technology/Federal University of Rio Grande do Norte, Natal 59078-900, Brazil*

Received 20 October 2021; accepted 2 December 2021
Available online 08 December 2021

KEYWORDS

Heterogeneous catalyst;
Deconvolution method;
Waste cooking oil;
Alternative silica;
Sodium potassium silicates;
Biodiesel

Abstract Heterogeneous catalysts, named SPS (sodium potassium silicates), were synthesized with an alternative silica (MPI silica) obtained from beach sand. In this work, the MPI was modified with NaOH and KOH producing silicate-based catalyst for biodiesel synthesis from waste cooking oil (WCO). The obtained catalyst was characterized by XRD, CO_2-TPD, the Hammett basicity test, XRF, FESEM, EDX, FTIR and TG/DTG. The results confirmed the presence of K_2O/Na_2O oxides and their silicates, the main active sites responsible for the catalytic action. CO_2-TPD and the Hammett basicity data suggested the presence of weak, medium and strong basic sites. Biodiesel yield was about 92% and the SPS catalyst was reused for five cycles. The biodiesel conversion by NMR ^1H was about 93.89%. The DTG deconvolution revealed the decomposition of four typical biodiesel compounds ($R^2 = 0.9987$). The method applied for the WCO biodiesel production using SPS catalyst represents an environmentally friendly process, based on low-cost material and reuse of waste biomass.

Abbreviations: WCO, Waste cooking oil; SPS, Sodium and potassium sicate

* Corresponding authors: Energetic Technologies Research Group, Institute of Chemistry and School of Science and Technology, Federal University of Rio Grande do Norte, Natal 59078-900, Brazil.
E-mail addresses: keversonoliveira@hotmail.com (K.G. de Oliveira), luciene_car@hotmail.com (L.S. de Carvalho).

Peer review under responsibility of King Saud University.

Production and hosting by Elsevier

1. Introduction

Renewable energy sources, that minimize environmental impact, have been the basis of several studies in the last few years to find aiming an alternative to substitute the use of fossil fuels. Low-cost materials have been used for biofuel production, which contribute to reducing the damage caused by fossil fuels (Sammah and Ghiaci, 2018). Confirming this trend, the global biodiesel production in 2020 was estimated at around 36.9 million metric tons (Huang et al., 2020). Furthermore

https://doi.org/10.1016/j.arabjc.2021.103603
1878-5352

several studies have shown a market recovery in 2021, reaching the average production of 46 billion liters between 2023 and 2025 (International Energy Agency, 2020).

Biodiesel is a sustainable alternative to the demand of diesel usage which enables of decrease pollutants emission such as CO_2 (Mostafa and El-Gendy, 2017). This product can be classified as first-generation (derived from edible vegetable oils), second-generation (non-edible raw material or waste), and third-generation (algae biomass) biodiesel (Ramos et al., 2019). Some studies have been developed to optimize the synthesis process of biofuel, which normally proceeds by triacylglyceride transesterification with methanol or ethanol in the presence of catalysts that may have basic (NaOH, KOH, CH_3ONa and CH_3OK) or acid (H_2SO_4, H_3PO_4, HCl, and R — SO_3H) characteristics. However, these catalysts are more difficult to be separated and reused, in addition to being able to cause secondary reactions such as saponification (Farias et al., 2020; Manríquez-Ramírez et al., 2013).

In this context, heterogeneous catalysts have been applied for the biodiesel production, because they minimize the problems arising from the use of homogeneous catalysts, enabling a more efficient purification process (Luo et al., 2017; Niju et al., 2016). Several feedstock have been used in this catalysts production, such as plant and animal-derived compounds, metallurgical/mining industrial residues and natural clays. (Rizwanul Fattah et al., 2020). A few heterogeneous catalysts used to produce biodiesel are sodium silicate for soybean biodiesel (Guo et al., 2012), silica coated on Fe_3O_4 magnetic nanoparticles (Thangara et al., 2019), ground alkaline metals for palm biodiesel (Salamatinia et al., 2013), K_2O/NaX and

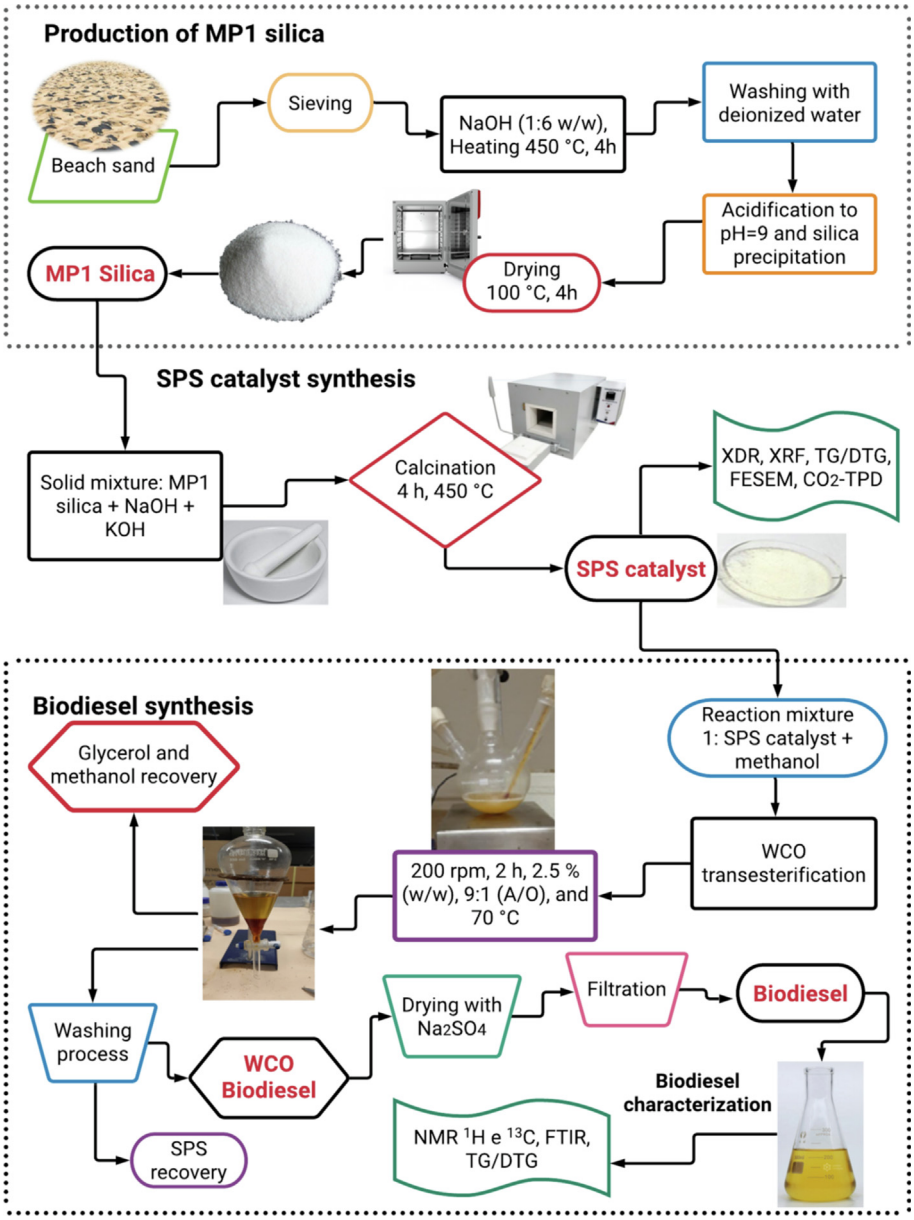

Fig. 1 Simplified flow diagram of the overall methodology for catalyst preparation and biodiesel production from waste cooking oil (WCO).

Na_2O/NaX for Safflower biodiesel (Muciño et al., 2014), and alkaline metal catalyst (Li, Na and K) supported on rice husk silica for WCO biodiesel (Hindryawati et al., 2014).

Search for greater economic viability and reduction in the environmental impact of the biodiesel production process has motivated the usage of waste biomass (Gollakota et al., 2019). Thereby, the WCO may be a good choice since it is cheaper than the refined oil (Vela et al., 2020), non edible and it can reduce the environmental impact caused by its inappropriate discarding (Gollakota et al., 2019), as around 5 million tons of refined oil are consumed per year around the world (Tan et al., 2019). Meanwhile, WCO normally presents relatively high free fatty acids that require pretreatment by esterification, before the transesterification, in order to avoid the soap formation (Ding et al., 2012).

This work contributes to the development of novel heterogeneous catalysts (SPS, sodium potassium silicates) for producing biodiesel from WCO. Moreover, the alternative MPI silica was applied for the catalysts production after its modification with alkali hydroxides. Despite being a waste material, there was no need of WCO pre-treatment (acid esterification) and the direct transesterification was accomplished using SPS. In this process, it was possible to use the catalyst for five reaction cycles. The use of waste raw material (WCO) for biodiesel production and a natural source (MPI silica) for the catalyst preparation are relevant factors that ensure low-cost and environmentally friendly biodiesel production process.

2. Materials and methods

2.1. Reagents

Waste cooking soybean oil was obtained from Brazilian restaurant. The other reagents were: Silica beach sand (MPI silica); Hydrochloric acid (HCl, Synth, 36.5%); Sodium hydroxide (NaOH, Vetec, 99%); Potassium hydroxide (KOH, Synth PA); Ethanol (C_2H_5OH, Dynamic PA, 96%); Sodium chloride (NaCl, Dynamic, 99%); Methanol (CH_3OH, Vetec, 99.8%); Sodium sulfate (Na_2SO_4, Vetec, 99%); Benzoic acid ($C_7H_6O_2$, Dynamic, 99.5%); Phenolphthalein ($C_{20}H_{14}O_4$, Vetec PA ACS) and Distilled water. The chemicals obtained were used as received.

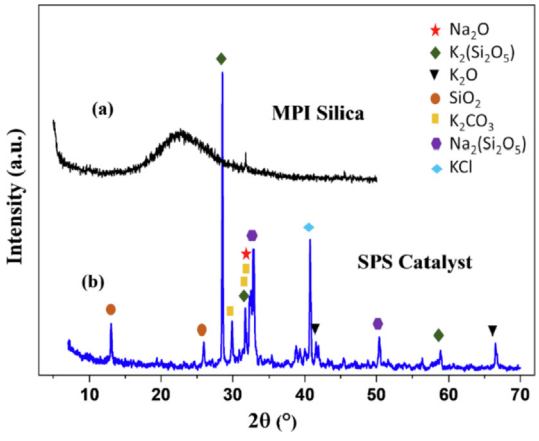

Fig. 2 XRD pattern of MPI silica and SPS catalyst.

2.2. Catalyst preparation and characterization

Amorphous silica MPI was synthesized from beach sand using a methodology developed in this research group and described by de Carvalho et al. (2015). In this work, the SPS catalysts were obtained by calcination of mixtures containing alkaline hydroxides (NaOH and KOH) and MPI silica, at 450 °C in a muffle furnace for 4 h. Different molar ratios of NaOH: KOH:MPI silica were used (1:1:1; 2:1:1; 1:2:1, and 1:1:2), to produce the catalysts named SPS, SPS-1, SPS-2, and SPS-3 respectively. The obtained catalysts were applied in preliminary tests for the biodiesel production, using the following synthesis conditions: 3.5% (w/w, catalyst/WCO), 9:1 (molar ratio A/O), 2 h, and 70 °C.

The catalysts were characterized by various techniques. X-ray diffraction analyses (XRD) were performed using a Bruker D2 Phaser device (Bruker AXS, Madison, WI, USA) with CuKα radiation (λ = 1.5406 Å), 30 kV filament, 10 mA current, Ni filter and a LYNXEYE detector in the range from (2θ) 5 to 50° for MPI silica, and 5 to 70° for the catalysts. Elemental analysis was conducted on a Bruker S2 Ranger X-ray fluorescence (XRF) Spectrometer (Bruker AXS, Madison, WI, USA) using Pd or Ag radiation (max. power 50 W, max. voltage 50 kV, max. current 2 mA, XFlash® Silicon Drift Detector). Fourier transform infrared spectroscopy (FTIR) was accomplished in a Shimadzu IRAffinity-1 spectrometer (Columbia, MD, USA) with attenuated total reflectance (ATR). Spectrum analysis variation was in the range of 600–4000 cm^{-1} with a resolution of 4 cm^{-1} and 32 scans. The thermal analysis was performed in a thermo microbalance (TG-209-F1-Libra, Netzsch, Selb, Germany) using an alumina crucible for measuring 10 mg of the samples with a continuous heating rate of 10 °C min^{-1} in nitrogen ($N_{2(g)}$) purge gas at a flow rate of 20 mL min^{-1}.

The morphologies and chemical composition of catalysts were obtained using a field emission scanning electron microscope (FESEM, Auriga, Carl Zeiss, Oberkochen, BW, Germany) and energy dispersive X-ray spectroscopy (EDX, XFlash Detector 410-M, Madison, WI, USA), respectively.

The analysis of CO_2 desorption at programmed temperature (CO_2-TPD) consisted of weighing a 200 mg of the SPS catalyst. Next, the pre-treatment was performed with heating

Table 1 Elemental composition of MPI silica and SPS catalysts deduced from XRF analysis.

Elements	MPI silica (%)	SPS (%)	SPS-1 (%)	SPS-2 (%)	SPS-3 (%)
K_2O	0.06	48.51	37.57	66.71	16.02
Cl	1.43	9.60	6.86	5.29	12.67
SiO_2	90.52	20.90	24.10	14.01	56.22
P_2O_5	0.05	0.33	–	0.10	0.40
MgO	1.5	2.1	1.5	1.6	1.5
Na_2O	3.5	16.6	28.0	9.3	10.3
Fe_2O_3	0.19	0.18	0.12	0.17	0.26
Al_2O_3	2.25	1.22	1.24	1.36	1.71
SO_3	0.17	0.56	0.36	0.95	0.62
CaO	0.16	–	–	–	0.17
TiO_2	0.04	–	0.07	0.11	0.05
ZrO_2	0.03	–	0.03	0.31	0.01
ZnO	–	–	0.10	0.14	–

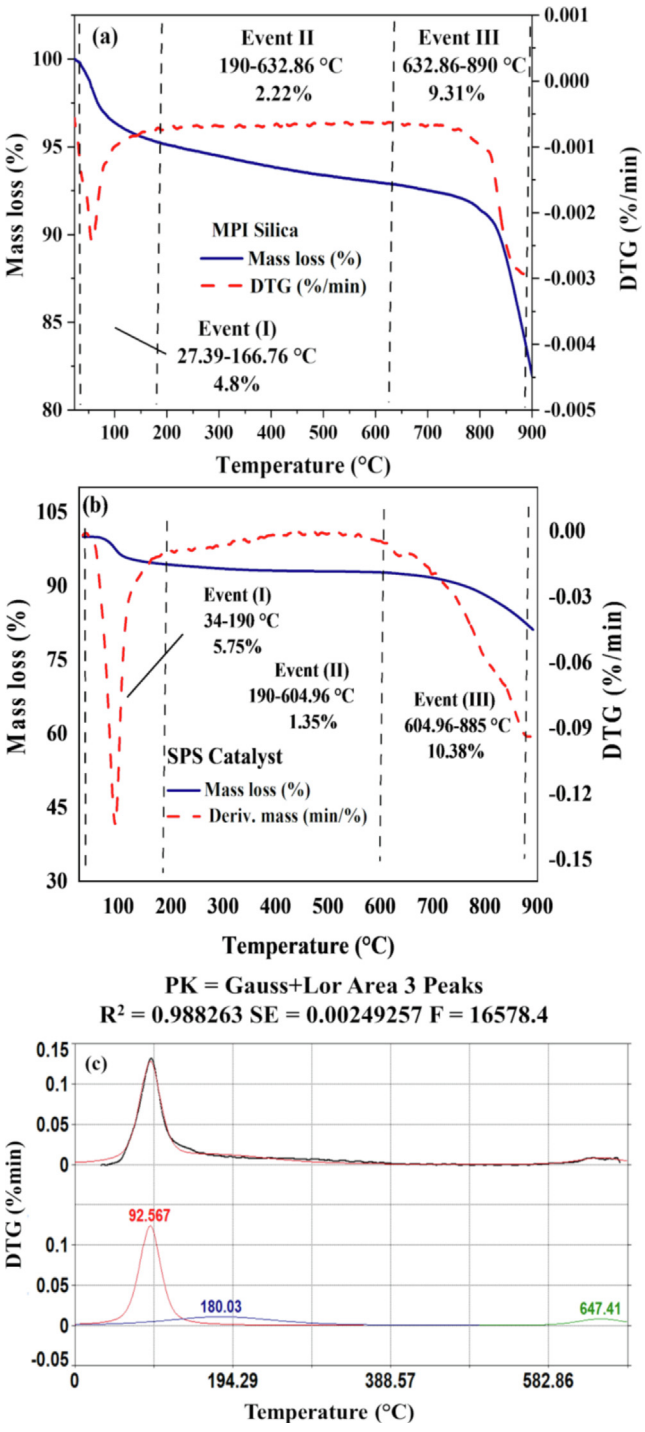

Fig. 3 TG/DTG analysis curves for MPI silica (a), SPS catalyst (b), and DTG deconvolution of SPS catalyst.

at 200 °C under a N_2 flow of 16 mL min^{-1} for 1 h. At the end of this period, the temperature was reduced to 60 °C and the CO_2 flow (16 mL min^{-1}) was inserted into the reaction line to start the adsorptive process for 30 min. The analysis was subsequently started in a He (g) atmosphere in the temperature range of 40 °C to 500 °C with a heating rate of 10 °C min^{-1} min under He (g) flow (16 mL min^{-1}). The desorbed CO_2 was then quantified by a thermal conductivity detector.

The deconvolution methodology was applied to the CO_2-TPD, and TG/DTG of catalyst and biodiesel using PeakFit 4.12 software (Systat Software, Inc., Berkshire, UK) by applying Gauss + Lorentz for better curve adjustment, Savitzky-Golay smoothing filter (< 20%) and linear baseline.

Hammett's basicity test was performed using the titration method with acid-base indicators. A phenolphthalein indicator ($H_- = 9.3$) and a 0.01 mol/L methanolic benzoic acid solution were used as the titrant for the experimental procedure. The Hammett basicity test consisted of stirring 0.15 g of the catalyst with 2 mL of methanolic indicator solution at a concentration of 0.1 mg mL^{-1} for 30 min at 300 rpm. The obtained data were then applied in Eq. (S1) and (S2) (all figures, tables and equations indicated with S are in the supplementary material) to calculate the number of basic sites from the basicity calculation.

Raman spectra were obtained using a confocal Raman microscope (LabHAM HR Evolution, HORIBA Scientific), with laser wavelength of 532 nm, grade: 600 gr mm^{-1}, laser power of 1% and scanning range 400–4000 cm^{-1}. N_2 adsorption–desorption isotherms at 77 K were used to determine the textural parameters of the SPS catalyst in a Micromeritics ASAP 2020 apparatus (Norcross, GA, USA). The specific surface area (S_{BET}) was calculated using the Brunauer – Emmett – Teller (BET) equation.

2.3. Preparation and characterization of biodiesel from WCO

Biodiesel was synthesized in three consecutive stages: (i) previous filtration of the WCO in a separating funnel to remove impurities; (ii) transesterification reaction at 70 °C with methanol and catalyst in a reflux reactor; and (iii) purification according to the methodology described in the literature (Fernandes et al., 2012), with adaptations. The time, catalyst concentration and molar ratio parameters were varied for synthesis optimization.

Hydrogen Nuclear Magnetic Resonance (NMR ^1H) and Carbon-13 (NMR ^{13}C) one-dimensional analyses were obtained by a Bruker Avance III HD NMR SPECT. 300 Spectrometer operating at frequencies of 300.13 MHz for hydrogen (^1H) and 75.47 MHz for carbon (^{13}C) respectively. The WCO and biodiesel were dissolved in deuterated chloroform ($CDCl_3$) in the proportion of 20 mg of sample to 0.5 mL of solvent. The chemical shifts (δ) were expressed in parts per million (ppm) and Tetramethylsilane (TMS) was used as an internal standard. Eq. (S3) was used to calculate the conversion of esters (Gohain et al., 2017).

The thermal analysis (TG/DTG) was accomplished in a thermo microbalance (TG-209-F1-Libra, Netzsch, Selb, Germany) using nitrogen ($N_{2(g)}$) as purge gas at a flow rate of 20 mL min^{-1}, alumina crucible, heating rate of 10 °C min^{-1}, 10 mg of sample and final temperature was 600 °C. The deconvolution was performed using the Peakfit v.4.12 software.

The physical–chemical properties were obtained under conditions for density at 20 °C and kinematic viscosity at 40 °C according to the American Society for Testing and Materials (ASTM) D4052 and D7042, respectively. The yields of the transesterification reactions were calculated using Eq. (S4) (Yang et al., 2016). The acidity index was obtained applying Eq. (S5) (AOCS, 2009).

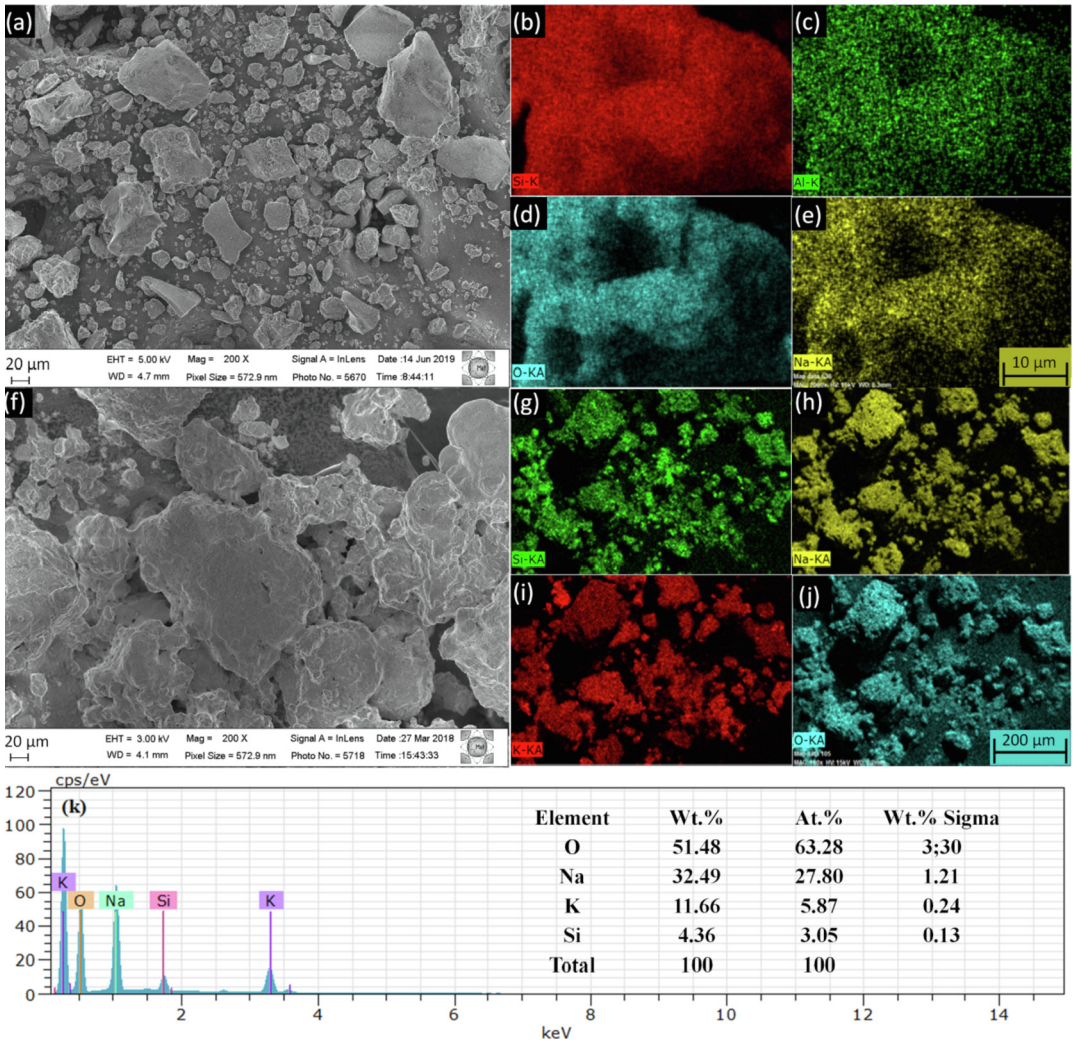

Fig. 4 (a) FESEM; (b–e) elemental mapping images of MPI silica and (f) FESEM, (g-j) mapping images, (k) and EDX spectrum of SPS catalyst.

2.4. Catalyst reuse

The regeneration was performed in three stages: (1) washing with mixture of hexane and ethanol (50 mL, 1:1 v/v) under stirring for 1 h, (2) soaking in a new mixture of hexane and ethanol (50 mL, 1:1 v/v) for 4 h to remove excess glycerol and waste cooking oil that could remain on its surface and (3) oven drying for 2 h at 150 °C. This procedure was repeated for five cycles.

The overall methodology employed in this research is presented in a simplified flow diagram depicted in Fig. 1.

3. Results and discussion

3.1. Preliminary tests for catalysts syntheses

The catalysts syntheses were performed with different proportions of MPI silica, NaOH, and KOH in order to evaluate the reaction yield under the reaction conditions described in Table S1. (S indicates supplementary material). The selected SPS catalyst was obtained with lower proportion (1:1:1) of the reagents, since the others did not significantly affect the reaction yield for WCO biodiesel production, Table S2. However, the concentrations of the species obtained by XRF that correspond to the oxides of the components showed differences related to the feed molar ratio (Do Nascimento-Dias et al., 2017), which probably occurred due to the utilization of sodium and potassium hydroxides that reacted with silica forming the metal silicates and producing the catalyst, with the possibility of varying the concentrations. In addition, it was possible to verify that pure silica did not have the ability to catalyse the reaction, indicating the need to modify its structure and composition.

3.2. Characterization of MPI silica and SPS catalyst

The XRD pattern for MPI silica (Fig. 2a) exhibited a broad peak centered at 2θ angle 22.8°, characteristic of an amorphous silica structure with the presence of short-range order in atomic clusters (Salakhum et al., 2018; Stanishevsky and Tchernov, 2019), the crystalline plane phases of the SPS cata-

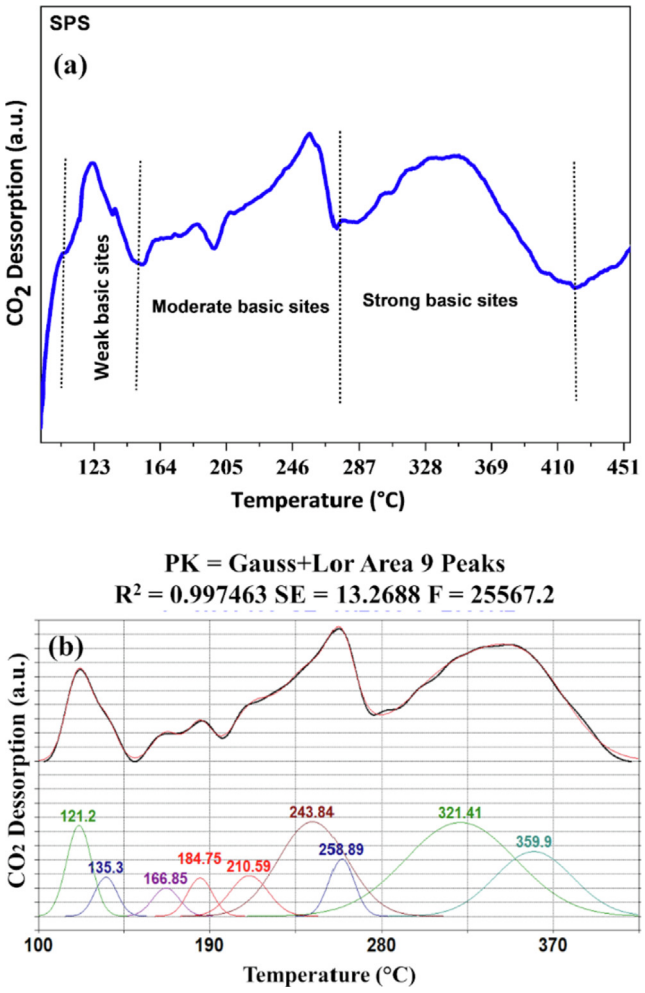

Fig. 5 CO_2-TPD deconvolution analysis for SPS catalyst.

lyst corresponding to Na_2O (2θ = 32.23°, ICSD 060435), KCl (2θ = 40.72°, ICSD 044281), $K_2(Si_2O_5)$ (2θ = 28.57°, 31.77° and 58.87°, ICSD 280480), K_2O (2θ = 41.50° and 66.53°, ICSD 060489), SiO_2 (2θ = 13.10° and 25.87°, ICSD 065497), K_2CO_3 (2θ = 29.87°, 31.75°, 31.77° and 66.47°, ICSD 000662) and $Na_2(Si_2O_5)$ (2θ = 32.80° and 50.47°, ICSD 080378) were shown in Fig. 2b indicating that the modification of the MPI silica to obtain catalytic sites was successful.

The XRF results for the SPS catalyst and MPI silica were described in Table 1and allowed to confirm the elements presence of found in the XRD phases, revealing the presence of alkali oxides as the main components of the produced SPS. These compounds have the ability to promote the catalytic activity of the transesterification reaction (Chouhan and Sarma, 2013), since mixed metal oxides are present as an interesting class of solid heterogeneous catalysts, allowing the association of the various oxide phases that promote appropriate characteristics for the reaction process (Lee et al., 2016).

FTIR spectra of MPI silica and SPS were presented in Fig. S1 and Table S3. For both materials the band at 1417 cm^{-1} indicates the existence of Na_2CO_3 formed by the reaction of sodium hydroxide with atmospheric CO_2 (Belmokhtar et al., 2016; Simanjuntak et al., 2014). The broadband in the region of 2500 and 3750 cm^{-1} may be attributed to OH groups from silanol and adsorbed water (Hindryawati et al., 2014). For MPI silica the band at 1314 cm^{-1} is associated with asymmetrical stretching of the siloxane (Si-O-Si) bonds (Hindryawati et al., 2014). Additional description of the SPS FTIR spectrum were provided in Table S3.

A comparison of both spectra, allowed observing a decrease in the intensity of the bands in the range of 3526 to 2451 cm^{-1} in MPI silica, probably due to moisture loss during the silica calcination to produce the SPS. Additionally, the decrease of a signal at 1606 cm^{-1} and disappearance of the band at 1314 cm^{-1}, in the SPS catalyst might have occurred due to a reaction of the silane's groups polycondensation during SPS preparation. The increase in intensity of the band at 1427 cm^{-1} is attributed to the carbonates formed after the treatment of MPI silica to produce SPS (Peyne et al., 2017). Moreover an enlargement of the peak at 1000 cm^{-1} (Si-O-Si group in the MPI silica) in the range of 1000–800 cm^{-1} is noted, which could be probably due to the overlap of some peaks present in the SPS. The changes in the silicon bands would be caused by depolymerization of the silica network by the potassium ions, which are network-modifying agents and may affect the number of atoms in the first coordination sphere of the atomic silicon (Puligilla et al., 2018).

The results of the thermogravimetric analysis for the MPI silica exhibited three main events characteristics of amorphous silica (Fig. 3a). The first event of mass loss (4.8%) occurred in the range of 27.39 °C to 190 °C, due to the removal of physisorbed water on the silica surface. The second mass loss event occurs over a wide temperature range of 190 to about 632.86 °C (mass loss of 2.22%), probably due to the condensation of less stable silanols and of silane into siloxane. The third event (9.31% of mass loss) starting at 632.86 °C may be attributed to the more stable silanols were dehydroxylated and condensed (De Carvalho et al., 2015; Kin et al., 2009).

The results of the thermal analysis for SPS, Fig. 3b, showed (I) a 5.75% of mass loss attributed to the water molecules adsorbed on the material (34–190 °C) and (II) a second mass loss event of 1.35% attributed to the silanols and silane into siloxane condensation, of the 190 °C to 604.96 °C, and (III) third mass loss event of 10.38%, release of water by condensation/polymerization of the Si-OH groups above 604.96 (He et al., 2010; Kin et al., 2009). The DTG deconvolution result of the SPS catalyst, Fig. 3c and Table S4 confirmed the three mass loss events verified in Fig. 3b. This shows the stability of the material after removing the water by heating for activating the catalyst.

The FESEM micrograph for the MPI silica revealed the presence of irregularly distributed particles (Fig. 4a). The EDX maps showed a homogeneous distribution of the elements Si, Al, O, and Na on the surface of the support (Fig. 4-b-e). FESEM micrograph for SPS (Fig. 4f) indicated larger irregular structures in relation to the image obtained for the MPI silica (Fig. 4a). Upon modification of MPI silica with alkali treatment and calcination the surface heterogeneity (with steps and kinks) and particle agglomeration are enhanced. The mapping images (Fig. 4g-j) demonstrated that there is good dispersion of the elements Si, Na, K, and O over the catalyst. The morphological changes in the silica MPI which acts as a support presented formation of the SPS catalyst by adding alkali metals and the adopted synthesis methodology. The EDX maps and spectra for both materials, SPS (Fig. 4k) and MPI silica (Fig. S2) are in agreement with the XRD (Fig. 2) and XRF results (Table 1).

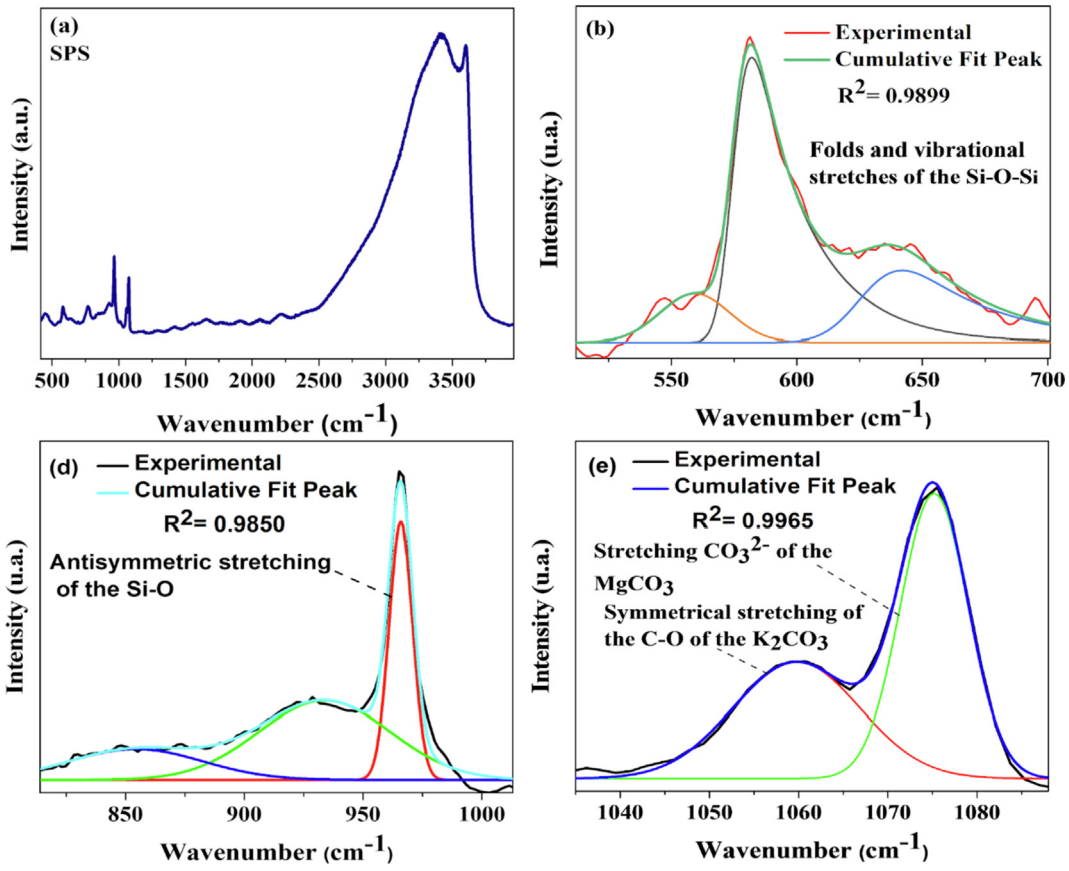

Fig. 6 Raman spectra of SPS catalyst.

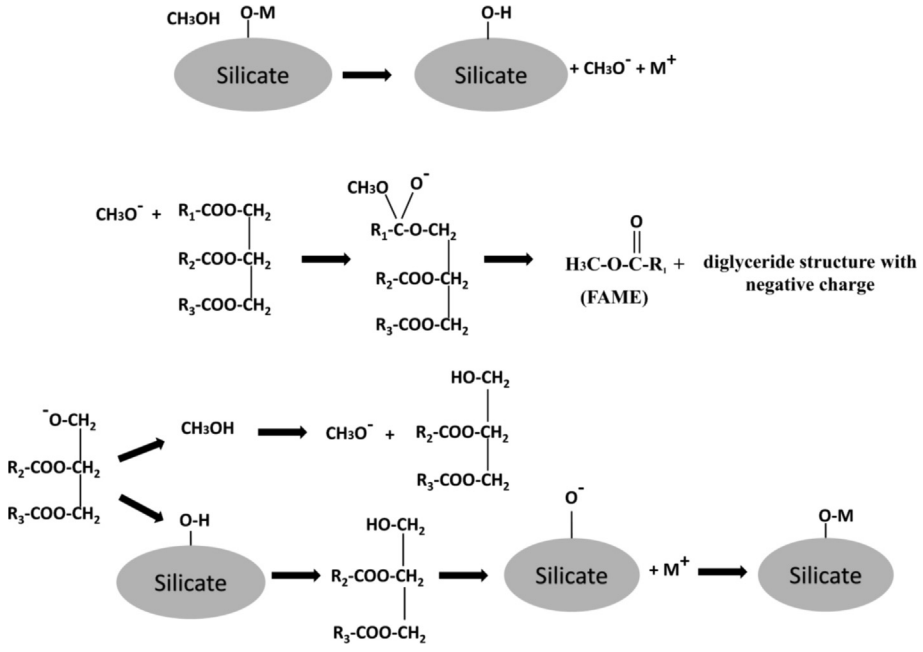

Fig. 7 Proposed mechanism for the H/M ion exchange of methanol with base sites of alkaline silicates.

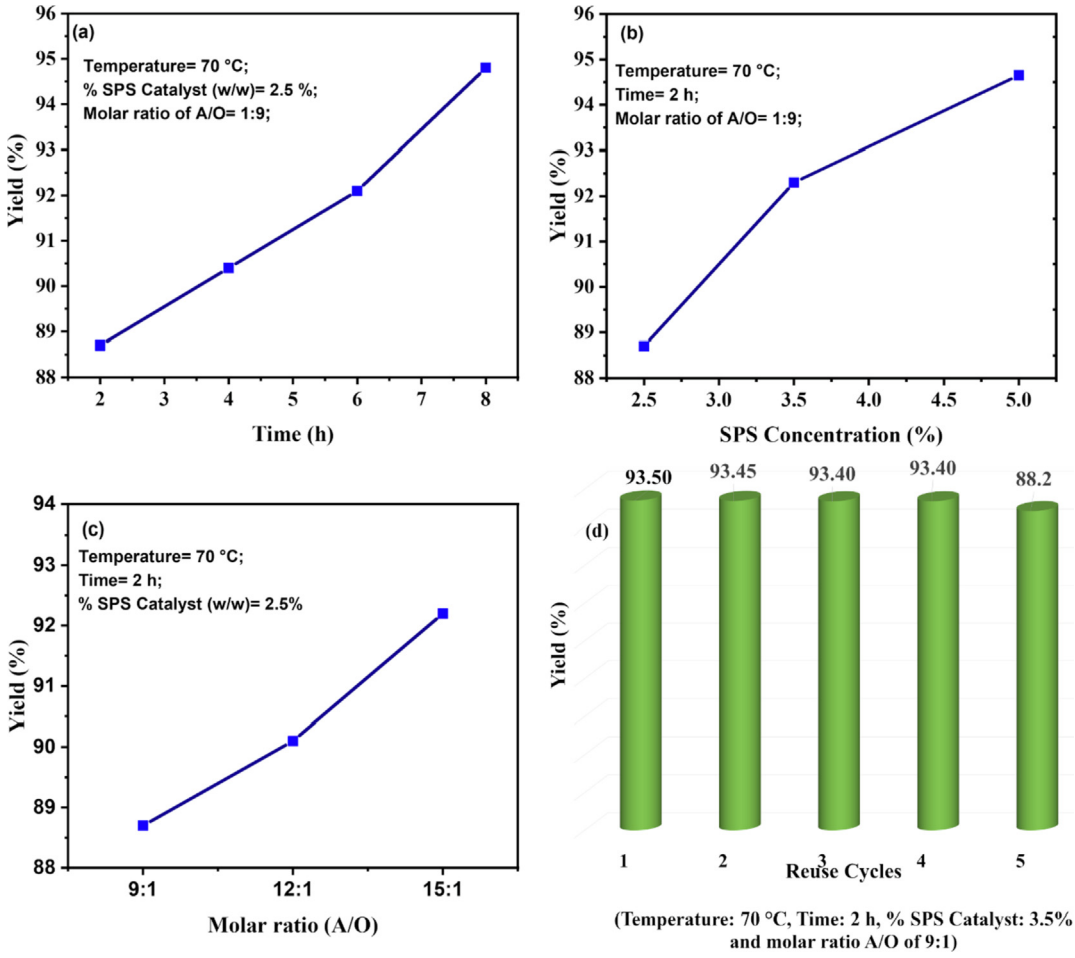

Fig. 8 Biodiesel yield (%)as a function of (a) time variation, (b) SPS concentration, (c) molar ratio of A/O and (d) reuse of the catalyst.

The CO_2-TPD results of SPS (Fig. 5a) exhibited several desorption peaks, indicating the presence of with weak (100. 67–149.71 °C), medium (149.71–273 °C) and strong (273–405 °C) basic sites, demonstrating the heterogeneity of the material (Eom et al., 2015).

The deconvolution of the CO_2-TPD (Fig. 5b and Table S5) enabled to verify that the largest proportion of basic sites are strong characteristic, composing about 51.9%, with 31.6% corresponding to sites of medium strength.

The results of the Hammett basicity test were positive to identify that SPS has basic sites in the range of $9.3 < H_- < 15$ of phenolphthalein (pKb = 9.8), corresponding to 3.2 mmol g^{-1} of the indicator, which denote the presence of a substantial quantity of active sites at alkaline pH in the SPS (Okoye et al., 2019). According to the specialized literature, sodium and potassium silicates have a basic strength above the phenolphthalein range (range $15 < H_- < 18.4$) (Hindryawati et al., 2014), justifying the catalytic capacity of the SPS catalyst (this study). The obtained results of basicity are consistent with those of CO_2-TPD.

In the Raman spectrum of SPS catalyst, Fig. 6, there were peaks in the range of 500–700 cm^{-1} that could be attributed to vibrational stretching and bend of the Si-O-Si (Santos et al., 2019; Partyka and Leśniak, 2016). At 965.20 cm^{-1} there was a peak that corresponds to the antisymmetric stretching of the Si-O bond (Zhu et al., 2019). At 1059.84 cm^{-1}, a peak of strong intensity was attributed to the symmetrical stretching of the C-O of the K_2CO_3 group (Ma et al., 2021). A peak at 1074.96 cm^{-1} was assigned to stretching CO_3^{2-} of the $MgCO_3$ (Williams et al., 1992).

The N_2 adsorption–desorption isotherms of SPS (Fig. S3) were classified as type III at relative pressures of $0.1 < P/P_o < 0.6$, and type IV(a) at $0.6 < P/P_o < 0.98$, with an H3 hysteresis cycle (Thommes et al., 2015). The specific surface area (S_{BET}) obtained for the SPS catalyst is 0.710 $m^2\ g^{-1}$ and the pore volume is 0.00421 $cm^3\ g^{-1}$. This demonstrates a sharp drop when compared to the MPI silica that presented S_{BET} of 33.54 $m^2\ g^{-1}$ and pore volume of 0.18 $cm^3\ g^{-1}$, according to Carvalho et al. (2015). This decrease may be associated with the addition of K^+ and Na^+ and also due to the particle agglomeration upon calcination as seen in FESEM images. Strong basic sites that may occlude the catalyst pores (Farias et al., 2011).

3.3. Proposed mechanism for biodiesel production

In accordance with the obtained XRD, XRF, and Raman results, three species make up the SPS catalyst: potassium carbonate, alkali metal oxides, and sodium and potassium silicates. In this work, a mechanism was proposed for biodiesel synthesis by transesterification reaction, adapted from Guo

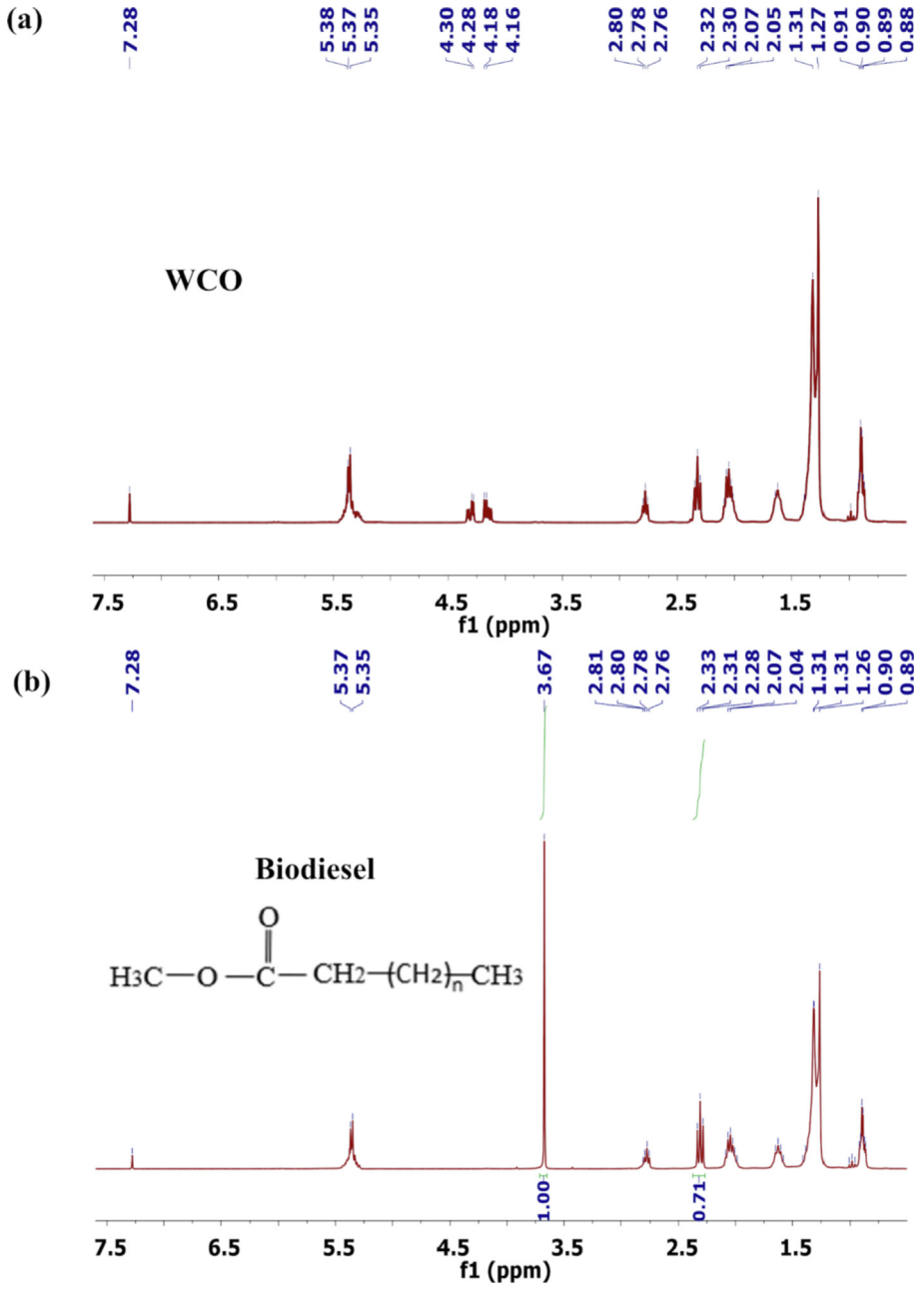

Fig. 9 ^{1}H NMR spectra (a) WCO and (b) biodiesel.

et al. (2012). This proposal is based on the silicate interactions (Fig. 7), in which the methanol approaches the catalyst surface favoring the ion exchange between the metal silicate (Na or K) and the hydrogen from the alcohol forming the methoxide. There is a subsequent nucleophilic attack of the methoxide on the carbonyl of the triglyceride forming the tetrahedral intermediate that after rearrangement results in the fatty acid methyl esters (FAME). Lastly, an intramolecular rearrangement of protons in the diglyceride occurs to stabilize the charge.

3.4. Biodiesel synthesis

3.4.1. Assessment of transesterification yield

The reaction yield (%) for the biodiesel synthesis (calculated by Eq. S4) was assessed at different conditions of time, molar ratio of alcohol to oil (A/O), SPS catalyst concentration and its reuse (Fig. 8). It was observed that the yield progressively increased with increase in time (Fig. 8a), catalyst concentration, and molar ratio of A/O (Fig. 8b-c), as determined through Eq. (S4). The tests for the SPS reuse revealed a good catalyst performance as the reaction yield was approximately the same during in the first four cycles, with a decrease only in the fifth cycle (Fig. 8d). The factors that most influenced the yield were time and A/O molar ratio from 12:1 to 15:1.

3.4.2. Biodiesel characterization

The ^{1}H NMR spectra for the waste cooking oil (WCO) (Fig. 9a) and biodiesel (Fig. 9b) were obtained with the purpose of evaluating the biodiesel purity and the conversion to esters in the SPS-catalysed transesterification reaction. The

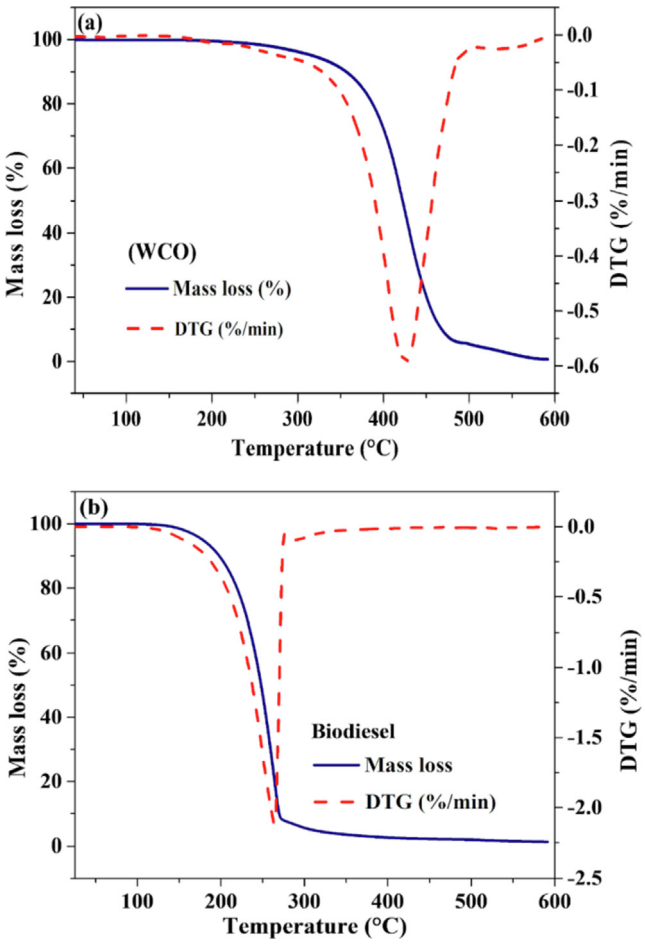

Fig. 10 TG/DTG curves of (a) WCO and (b) biodiesel produced from waste cooking oil using SPS catalyst.

conversion may be confirmed by the disappearance of the peaks at 4.1–4.3 ppm, attributed to hydrogen from triglycerides (WCO) (Ruschel et al., 2016), and the appearing of a signal at 3.7 ppm due to hydrogen from methoxy groups of methyl esters (biodiesel) (Gohain et al., 2017), resulting in a conversion of around 93.89% (Eq.(S3)). In addition, absence of contaminants is observed.

In the ^{13}C NMR spectra of WCO and biodiesel (Fig. S4), carboxyl ester group (signals at 174.3 and 54.43 ppm) and olefinic groups (unsaturated methyl ester, signals in the range of 130.18–129.73 ppm) respectively were observed (Fig. S4a). Furthermore, triglycerides peaks (CH-O and CH_2-O) are found between 68.88 and 61.77 ppm (Fig. S4a) (Tariq et al., 2011). A peak referring to methyl carbon appears at 14.9 ppm, while carbons of methylene groups (hydrocarbon chain) were observed in the range of 34.9–22.48 ppm (Fig. S4b) (Gohain et al., 2017). Comparing the results for WCO and biodiesel, it is possible to observe the disappearance of triglyceride peaks and the appearance of ester carbonyl signal (C-O) at 51.43 ppm in the ^{13}C NMR of biodiesel (Fig. S4b) (Tariq et al., 2011).

Thermal analysis of WCO and biodiesel produced from WCO (Fig. 10a and 10b) also confirmed the conversion and quality of biodiesel produced with the SPS catalyst, in agreement with the 1H NMR analysis (Fig. 9b). The DTG deconvolution method was performed on the DTG curve of biodiesel (Fig. S5 and Table S6) to evaluate its components. A mass loss event for WCO is observed in the range of 347–475 °C, (Fig. 10a) which corresponds to the decomposition of triglycerides while for the biodiesel the mass loss (Fig. 10b) occurs at lower temperatures in the region of 163 to 266 °C due to the decomposition of smaller molecules, corresponding to monoalkyl ester (Dantas et al., 2007; Misutsu et al., 2015). The SPS showed similar behaviour as other catalysts studied in the specific literature, which are described in Table 2.

It was possible to observe four components (Fig. S5) which corresponds to the observed mass loss in the TGA curve of biodiesel. Of these, three are attributed to monoalkyl ester, corresponding to 98% of the integrated area of DTG, and the other peak corresponds to oxidation products formed (about 2%) (Díaz-Ballote, 2018). It is possible to prove the synthesis occurrence via the thermal evaluation of biodiesel, which corroborates the ^{1}H and ^{13}C NMR results. The values calculated for the physicochemical properties such as density

Table 2 Comparison of the performance of SPS group of catalysts with literature reports.

Catalyst	Catalyst's preparation	Reaction conditions	Yeld (%)	Ref.
Pure silica	–	12 h, 70 °C, 3.5 (wt.%) catalyst, 400 rpm, A/O 9:1	Not converted	This work
SPS	MPI Silica + NaOH + KOH calcination, 4 h, 450 °C	2 h, 70 °C, 3.5 (wt.%) catalyst, 400 rpm, A/O 9:1	92.8	This work
SPS-1			93.6	
SPS-2			93.5	
SPS-3			93.7	
Na_2SiO_3	Dehydrated at 200 °C for 20 min and calcination, 2 h, 400 °C	Up to 4 h, 50–65 °C, 3–5 (wt.%) catalyst, A/O 1:3–1:15	57–99.6	Long et al., 2011.
Li, Na, K/Silicate	Silica/metallic ions, 2 h, 90 °C	1 h, 65 °C, 3 (wt.%) catalyst, A/O 9:1	96.5–98.2	Hindryawati, 2014.
Na_2SiO_3 (Sigma–Aldrich (Pty)	(direct use)	4 h, 64 °C, 2.5 wt% catalyst, A/O 6:1	57.92	Daramola et al., 2016
Na_2SiO_3 (Kermel Corp.)	Calcination, 2 h, 400 °C	1 h, 60 °C, 3 (wt.%) catalyst, A/O 7.5:1,	15–99	Guo et al., 2012.
K_2SiO_3	Silica from bamboo leaves + KOH, calcination, 2 h, 500 °C	2 h, 60 °C, 3 (wt.%) catalyst, A/O 9:1,	83.35	Manurung et al., 2019.
$KAlSiO_4$	$K_2O.3.9SiO_2$ + KOH + $Al(NO_3)_3$, calcination,4h, 1000–1200 °C	2–5 min, 120–180 °C, 3 (wt.%) catalyst,	20–54.4	Wen and Yan, 2011.

at 20 °C (0.890 g cm^{-3}), kinematic viscosity at 40 °C (5.061 mm^2 s^{-1}) and acidity index (between 0.355 and 0.155 mg KOH g^{-1}) were within the specifications of National Agency of Petroleum Natural Gas and Biofuels (ANP N° 45, 2014),. Characteristic bands of biodiesel were observed in the FTIR spectrum of biodiesel (Fig. S6). The band at 1736 cm^{-1}, was attributed to the elongation of the carbonyl bond; absorptions in the 1425–1447 cm^{-1} correspond to the asymmetric CH_3 flexion, and the bands in the range of 1188–1200 cm^{-1} correspond to O-CH_3 stretching (Mumtaz et al., 2012, De Morais et al., 2013).

4. Conclusions

The sodium potassium silicate (SPS) catalyst obtained in this work has a simple preparation method and may be considered of low-cost since it was produced from MPI silica derived from beach sand. In addition, exhibited high catalytic activity for biodiesel production for the conversion of waste oil (WCO) without previous of free fatty acids esterification. The efficiency of the catalyst synthesis method was verified by the XRD and XRF results, as well as the deconvolution method using the CO_2-TPD result to evaluate the strength of basic catalyst sites. The biodiesel production process involving heterogenous catalysis showed some advantage as the purification steps are more efficient than the homogeneous one, reducing mainly the amount of waste water. On the other hand, the reuse cycles of the catalyst indicate the possibility of its application in industrial scale. The reaction time was the most decisive parameter for the biodiesel yield (92%) and its high conversion (93.89%) can be verified by the ^{1}H NMR results. The spectroscopic, thermal analysis, and physicochemical data suggest the biodiesel from WCO was suitable for use as fuel.

Funding

This research was funded by Higher Education Improvement of Coordination Personnel - Brazil (CAPES) - Funding Code 001.

CRediT authorship contribution statement

Keverson G. de Oliveira: Writing – original draft, Conceptualization, Investigation, Formal analysis. **Ramoni R.S. de Lima:** Conceptualization, Investigation, Writing – review & editing, Formal analysis. **Clenildo de Longe:** Investigation, Writing – review & editing. **Tatiana de C. Bicudo:** Investigation, Writing – review & editing. **Rafael V. Sales:** Investigation. **Luciene S. de Carvalho:** Supervision, Writing – review & editing.

Declaration of Competing Interest

The authors declare that they have no known competing financial interests or personal relationships that could have appeared to influence the work reported in this paper.

Acknowledgement

The authors acknowledge the support provided by the Post-Graduate Chemistry Program (PPGQ/UFRN), the Energetic Technologies Research Group (GPTEN), and the Central Analitica (IQ/UFRN). This study was partly financed by the Coordenação de Aperfeiçoamento de Pessoal de Nível Superior – Brasil (CAPES) – Finance Code 001.

References

AOCS Official Method Cd 3d-63: Acid Value In: AOCS. 6. ed. Official methods and recommended practices of the American Oil Chemists' Society. Champaign: American Oil Chemists' Society, 2009. ISSN 2177-4420. https://www.infoteca.cnptia.embrapa.br/infoteca/bitstream/doc/1005866/1/CIT14.pdf. Acessed: 02. Feb.2021.

ASTM D4052-18a, Standard Test Method for Density, Relative Density, and API Gravity of Liquids by Digital Density Meter, ASTM International, West Conshohocken, PA, 2018, https://www.astm.org/Standards/D4052. Acessed: 02. Feb.2021.

ASTM D7042-21, Standard Test Method for Dynamic Viscosity and Density of Liquids by Stabinger Viscometer (and the Calculation of Kinematic Viscosity), ASTM International, West Conshohocken, PA, 2021, https://www.astm.org/Standards/D7042. Acessed: 02. Feb.2021.

Belmokhtar, N., Ben Allal, L., Lamrani, S., 2016. Effect of Na2SiO3/NaOH mass ratio on the development of structure of an industrial waste-based geopolymer. J. Mater. Environ. Sci. 7, 390–396. http://www.jmaterenvironsci.com/Document/vol7/vol7_N2/42-JMES-Belmokhtar-2016.pdf . Acessed: 02. Feb.2021.

Chouhan, A.P.S., Sarma, A.K., 2013. Biodiesel production from Jatropha curcas L. oil using Lemna perpusilla Torrey ash as heterogeneous catalyst. Biomass Bioenergy 55, 386–389. https://doi.org/10.1016/j.biombioe.2013.02.009.

Dantas, M.B., Conceição, M.M., Fernandes, V.J., Santos, N.A., Rosenhaim, R., Marques, A.L.B., Santos, I.M.G., Souza, A.G., 2007. Thermal and kinetic study of corn biodiesel obtained by the methanol and ethanol routes. J. Therm. Anal. Calorim. 87, 835–839. https://doi.org/10.1007/s10973-006-7780-2.

Daramola, M.O., Mtshali, K., Senokoane, L., Fayemiwo, O.M., 2016. Influence of operating variables on the transesterification of waste cooking oil to biodiesel over sodium silicate catalyst: a statistical approach. J. Taibah Univ. Sci. 10, 675–684. https://doi.org/10.1016/j.jtusci.2015.07.008.

De Carvalho, L.S., Silva, E., Andrade, J.C., Silva, J.A., Urbina, M., Nascimento, P.F., Carvalho, F., Ruiz, J.A., 2015. Low-cost mesoporous adsorbents amines-impregnated for CO2 capture. Adsorption 21, 597–609. https://doi.org/10.1007/s10450-015-9710-8.

De Morais, V.S., De Castro, E.V.R., Carneiro, M.T.W.D., Brandão, G.P., Júnior, R.F., De Sena, D.R., 2013. Cor astm: Um método simples e rápido para determinar a qualidade do biodiesel produzido a partir de óleos residuais de fritura. Quim. Nova 36, 587–592. https://doi.org/10.1590/S0100-40422013000400018.

Díaz-Ballote, L., 2018. Thermogravimetric approach for assessing the oxidation level of a biodiesel sample. Quim. Nova 41 (5), 492–496. https://doi.org/10.21577/0100-4042.20170199.

Ding, J., Xia, Z., Lu, J., 2012. Esterification and deacidification of a waste cooking oil (TAN 68.81 mg KOH/g) for biodiesel production. Energies 5, 2683–2691. https://doi.org/10.3390/en5082683.

Do Nascimento-Dias, B.L., Oliveira, D.F., dos Anjos, M.J., 2017. The utilization and multidisciplinary relevance of X-ray spectroscopy. Rev. Bras. Ensino Fis. 39. https://doi.org/10.1590/1806-9126-RBEF-2017-0089.

Eom, H.J., Kim, M.S., Lee, D.W., Hong, Y.K., Jeong, G., Lee, K.Y., 2015. Zirconia catalysts (ZrO2 and Na-ZrO2) for the conversion of phenethyl phenyl ether (PPE) in supercritical water. Appl. Catal. A Gen. 493, 149–157. https://doi.org/10.1016/j.apcata.2014.12.052.

Farias, A.F.F., de Araújo, D.T., da Silva, A.L., Leal, E., Pacheco, J.G. A., Silva, M.R., Kiminami, R.H.G.A., Costa, A.C.F.d.M., 2020.

Evaluation of the catalytic effect of ZnO as a secondary phase in the Ni0.5Zn0.5Fe2O4 system and of the stirring mechanism on biodiesel production reaction. Arab. J. Chem. 13, 5788–5799. https://doi.org/10.1016/j.arabjc.2020.04.016.

Farias, F.E.M., Neto, R.C.R., Baldanza, M.A.S., Schmal, M., Fernandes, F.A.N., 2011. Effect of K promoter on the structure and catalytic behavior of supported iron-based catalysts in Fischer-Tropsch synthesis. Brazilian J. Chem. Eng. 28, 495–504. https://doi.org/10.1590/S0104-66322011000300015.

Fernandes, D.M., Serqueira, D.S., Portela, F.M., Assunção, R.M.N., Munoz, R.A.A., Terrones, M.G.H., 2012. Preparation and characterization of methylic and ethylic biodiesel from cottonseed oil and effect of tert-butylhydroquinone on its oxidative stability. Fuel 97, 658–661. https://doi.org/10.1016/j.fuel.2012.01.067.

Gohain, M., Devi, A., Deka, D., 2017. Industrial Crops & Products Musa balbisiana Colla peel as highly e ff ective renewable heterogeneous base catalyst for biodiesel production. Ind. Crop. Prod. 109, 8–18. https://doi.org/10.1016/j.indcrop.2017.08.006.

Gollakota, A.R.K., Volli, V., Shu, C.M., 2019. Transesterification of waste cooking oil using pyrolysis residue supported eggshell catalyst. Sci. Total Environ. 661, 316–325. https://doi.org/10.1016/j.scitotenv.2019.01.165.

Guo, F., Wei, N.N., Xiu, Z.L., Fang, Z., 2012. Transesterification mechanism of soybean oil to biodiesel catalyzed by calcined sodium silicate. Fuel 93, 468–472. https://doi.org/10.1016/j.fuel.2011.08.064.

He, P., Jia, D., Wang, M., Zhou, Y., 2010. Effect of cesium substitution on the thermal evolution and ceramics formation of potassium-based geopolymer. Ceram. Int. 36, 2395–2400. https://doi.org/10.1016/j.ceramint.2010.07.015.

Hindryawati, N., Maniam, G.P., Karim, M.R., Chong, K.F., 2014. Transesterification of used cooking oil over alkali metal (Li, Na, K) supported rice husk silica as potential solid base catalyst. Eng. Sci. Technol. an Int. J. 17, 95–103. https://doi.org/10.1016/j.jestch.2014.04.002.

Huang, C.C., Ho, S.H., Chang, J.S., Gao, P.J., 2020. A sulfated/chlorinated Sr-Fe composite oxide as a novel solid and reusable superacid catalyst for oleic acid esterification. New J. Chem. 44, 13669–13684. https://doi.org/10.1039/d0nj00525h.

International Energy Agency, 2020, *Renewables 2020*, IEA, Paris. https://www.iea.org/reports/renewables-2020. Accessed: 02. sep.2021.

Lee, H.V., Juan, J.C., Yun Hin, T.Y., Ong, H.C., 2016. Environment-friendly heterogeneous alkaline-Based mixed metal oxide catalysts for biodiesel production. Energies 9 (8). https://doi.org/10.3390/en9080611.

Long, Y.D., Guo, F., Fang, Z., Tian, X.F., Jiang, L.Q., Zhang, F., 2011. Production of biodiesel and lactic acid from rapeseed oil using sodium silicate as catalyst. Bioresour. Technol. 102, 6884–6886. https://doi.org/10.1016/j.biortech.2011.04.007.

Luo, Y., Mei, Z., Liu, N., Wang, H., Han, C., He, S., 2017. Synthesis of mesoporous sulfated zirconia nanoparticles with high surface area and their applies for biodiesel production as effective catalysts. Catal. Today 298, 99–108. https://doi.org/10.1016/j.cattod.2017.05.047.

Ma, Y., Yan, W., Sun, Q., Liu, X., 2021. Raman and infrared spectroscopic quantification of the carbonate concentration in K2CO3 aqueous solutions with water as an internal standard. Geosci. Front. 12, 1018–1030. https://doi.org/10.1016/j.gsf.2020.03.002.

Manríquez-Ramírez, M., Gómez, R., Hernández-Cortez, J.G., Zúñiga-Moreno, A., Reza-San Germán, C.M., Flores-Valle, S.O., 2013. Advances in the transesterification of triglycerides to biodiesel using MgO-NaOH, MgO-KOH and MgO-CeO_2 as solid basic catalysts. Catal. Today 212, 23–30. https://doi.org/10.1016/j.cattod.2012.11.005.

Manurung, R., Siregar, H., Zuhri, R.R.S., 2019. Synthesis and characterization of K-Silica catalyst based bamboo-leaves for transesterification reaction. AIP Conf. Proc. 2085. https://doi.org/10.1063/1.5095047.

Misutsu, M.Y., Cavalheiro, L.F., Ricci, T.G., Viana, L.H., de Oliveira, S.C., Machulek, A., de Oliveira, L.C.S., 2015. Thermoanalytical methods in verifying the quality of biodiesel. Biofuels – Status Perspect. https://doi.org/10.5772/59479.

Mostafa, S.S.M., El-Gendy, N.S., 2017. Evaluation of fuel properties for microalgae Spirulina platensis bio-diesel and its blends with Egyptian petro-diesel. Arab. J. Chem. 10, S2040–S2050. https://doi.org/10.1016/j.arabjc.2013.07.034.

Muciño, G.G., Romero, R., Ramírez, A., Martínez, S.L., Baeza-Jiménez, R., Natividad, R., 2014. Biodiesel production from used cooking oil and sea sand as heterogeneous catalyst. Fuel 138, 143–148. https://doi.org/10.1016/j.fuel.2014.07.053.

Mumtaz, M.W., Adnan, A., Anwar, F., Mukhtar, H., Raza, M.A., Ahmad, F., Rashid, U., 2012. Response surface methodology: an emphatic tool for optimized biodiesel production using rice bran and sunflower oils. Energies 5, 3307–3328. https://doi.org/10.3390/en5093307.

National Agency of Petroleum Natural Gas and Biofuels (ANP, 2014). Ranp 45 - 2014. https://www.legisweb.com.br/legislacao/?id=274064.Acessed: 02. Feb.2021.

Niju, S., Meera Sheriffa Begum, K.M., Anantharaman, N., 2016. Enhancement of biodiesel synthesis over highly active CaO derived from natural white bivalve clam shell Enhancement of biodiesel synthesis over highly active CaO. Arab. J. Chem. 9, 633–639. Doi: 10.1016/j.arabjc.2014.06.006.

Okoye, P.U., Wang, S., Xu, L., Li, S., Wang, J., Zhang, L., 2019. Promotional effect of calcination temperature on structural evolution, basicity, and activity of oil palm empty fruit bunch derived catalyst for glycerol carbonate synthesis. Energy Convers. Manage. 179, 192–200. https://doi.org/10.1016/j.enconman.2018.10.013.

Partyka, J., Leśniak, M., 2016. Raman and infrared spectroscopy study on structure and microstructure of glass-ceramic materials from SiO2-Al2O3-Na2O-K2O-CaO system modified by variable molar ratio of SiO2/Al2O3. Spectrochim. Acta - Part A Mol Biomol. Spectrosc. 152, 82–91. https://doi.org/10.1016/j.saa.2015.07.045.

Peyne, J., Gautron, J., Doudeau, J., Joussein, E., Rossignol, S., 2017. Influence of silicate solution preparation on geomaterials based on brick clay materials. J. Non. Cryst. Solids 471, 110–119. https://doi.org/10.1016/j.jnoncrysol.2017.05.017.

Puligilla, S., Chen, X., Mondal, P., 2018. Understanding the role of silicate concentration on the early-age reaction kinetics of a calcium containing geopolymeric binder. Constr. Build. Mater. 191, 206–215. https://doi.org/10.1016/j.conbuildmat.2018.09.184.

Ramos, M., Dias, A.P.S., Puna, J.F., Gomes, J., Bordado, J.C., 2019. Biodiesel production processes and sustainable raw materials. Energies 12, 4408. https://doi.org/10.3390/en12234408.

Rizwanul Fattah, I.M., Ong, H.C., Mahlia, T.M.I., Mofijur, M., Silitonga, A.S., Ashrafur Rahman, S.M., Ahmad, A., 2020. State of the art of catalysts for biodiesel production. Front. Energy Res. 8. https://doi.org/10.3389/fenrg.2020.00101.

Ruschel, C.F.C., Ferrão, M.F., Dos Santos, F.P., Samios, D., 2016. Otimização do Processo de Transesterificação em Duas Etapas para produção de biodiesel. Quim. Nova 39, 267–272. https://doi.org/10.5935/0100-4042.20160018.

Salakhum, S., Yutthalekha, T., Chareonpanich, M., Limtrakul, J., Wattanakit, C., 2018. Synthesis of hierarchical faujasite nanosheets from corn cob ash-derived nanosilica as efficient catalysts for hydrogenation of lignin-derived alkylphenols. Microporous Mesoporous Mater. 258, 141–150. https://doi.org/10.1016/j.micromeso.2017.09.009.

Salamatinia, B., Hashemizadeh, I., Abdullah, A.Z., 2013. Alkaline earth metal oxide catalysts for biodiesel production from Palm oil: elucidation of process behaviors and modeling using response surface methodology. Iran. J. Chem. Chem. Eng. 32, 113–126. https://doi.org/10.30492/IJCCE.2013.5911.

Sammah, N., Ghiaci, M., 2018. Heterogenization of a homogenous catalyst: Synthesis and characterization of imidazolium ionene/OH-@SiO2 as an efficient basic catalyst for biodiesel production. New J. Chem. 42, 67–75. https://doi.org/10.1039/c7nj03285d.

Santos, A., Menezes, D., Ellena, J., Andrade, M., 2019. Aplicação Da Espectroscopia Raman Na Caracterização De Minerais Pertencentes a Uma Geocoleção. Quim. Nova 42, 489–496. https://doi.org/10.21577/0100-4042.20170358.

Simanjuntak, W., Sembiring, S., Zakaria, W.A., Pandiangan, K.D., 2014. The use of carbon dioxide released from coconut shell combustion to produce Na2CO3. Makara J. Sci. 18, 65–70. https://doi.org/10.7454/mss.v18i3.3717.

Stanishevsky, A., Tchernov, J., 2019. Mechanical and transport properties of fibrous amorphous silica meshes and membranes fabricated from compressed electrospun precursor fibers. J. Non. Cryst. Solids 525,. https://doi.org/10.1016/j.jnoncrysol.2019.119653 119653.

Tan, J., Zhang, S., Lu, T., Li, R., Zhong, T., Zhu, X., 2019. Design and synthesis of ethoxylated esters derived from waste frying oil as anti-ultraviolet and efficient primary plasticizers for poly(vinyl chloride). J. Clean. Prod. 229, 1274–1282. https://doi.org/10.1016/j.jclepro.2019.04.395.

Tariq, M., Ali, S., Ahmad, F., Ahmad, M., Zafar, M., Khalid, N., Khan, M.A., 2011. Identification, FT-IR, NMR (1H and 13C) and GC/MS studies of fatty acid methyl esters in biodiesel from rocket seed oil. Fuel Process. Technol. 92, 336–341. https://doi.org/10.1016/j.fuproc.2010.09.025.

Thangaraj, B., Jia, Z., Dai, L., Liu, D., Du, W., 2019. Effect of silica coating on Fe3O4 magnetic nanoparticles for lipase immobilization and their application for biodiesel production. Arab. J. Chem. 12, 4694–4706. https://doi.org/10.1016/j.arabjc.2016.09.004.

Thommes, M., Kaneko, K., Neimark, A.V., Olivier, J.P., Rodriguez-Reinoso, F., Rouquerol, J., Sing, K.S.W., 2015. Physisorption of gases, with special reference to the evaluation of surface area and pore size distribution (IUPAC Technical Report). Pure Appl. Chem. 87, 1051–1069. https://doi.org/10.1515/pac-2014-1117.

Vela, M.A.F., Acevedo-Páez, J.C., Urbina-Suárez, N., Basto, Y.A.R., González-Delgado, Á.D., 2020. Enzymatic transesterification ofwaste frying oil from local restaurants in east colombia using a combined lipase system. Appl. Sci. 10. https://doi.org/10.3390/app10103566.

Wen, G., Yan, Z., 2011. Transesterification of soybean oil to biodiesel over kalsilite catalyst. Front. Chem. Eng. China 5, 325–329. https://doi.org/10.1007/s11705-010-0574-x.

Williams, Q., Collerson, B., Knittle, E., 1992. Vibrational spectra of magnesite (MgCO3) and calcite-III at high pressures. Am. Mineral. 77, 1158–1165. (13) (PDF) Espectro vibracional de magnesite ($MgCO_3$) e calcita-III em altas pressões (researchgate.net). Accessed: 02. sep.2021.

Yang, J., Astatkie, T., He, Q.S., 2016. A comparative study on the effect of unsaturation degree of camelina and canola oils on the optimization of bio-diesel production. Energy Rep. 2, 211–217. https://doi.org/10.1016/j.egyr.2016.08.003.

Zhu, J.H., Hou, Y., Zheng, W.W., Zhang, G.H., Chou, K.C., 2019. Influences of Na2O, K2O and Li2O additions on electrical conductivity of $CaO–SiO_2–(Al_2O_3)$ melts. ISIJ Int. 59, 1947–1955. https://doi.org/10.2355/isijinternational.ISIJINT-2019-197.